An Investigation of Shear Instability in a Shallow Water Part II. Numerical experiment

By Takehiko Satomura

Geophysical Institute, Tokyo University, Tokyo 113
(Manuscript received 27 July 1981, in revised form 18 September 1981)

Abstract

Using a channel model in a shallow water, we numerically consider characteristics of finite-amplitude gravity waves which were found to be unstable waves in a constant shear flow by the linear analysis. Numerical integration is performed at Froude number equals to five for both inviscid and viscous case. In the inviscid run, it is shown that the first appeared mode has the growth rate and the structure which are the same as those expected from the linear analysis. Energy budget shows that disturbances extract their energy from the additional part of the mean kinetic energy as in the linear analysis.

In the viscous run (Re=3000), it is shown that disturbance energy reaches a quasi-steady state. Energy budget shows that energy is supplied to the mean kinetic energy, converted to the eddy kinetic energy, and then dissipated by the viscosity acting on the disturbances. Momentum budget indicates that these gravity waves can mix the averaged momentum permanently.

At a later stage of time integration, the disturbance energy oscillates. A linear stability analysis for the quasi-steady state is examined, and it shows that the oscillation is produced by unstable sub-harmonics.

Shape of disturbance depth near the boundaries and change of mean depth are also discussed.

1. Introduction

In one of previous papers (Satomura, 1981a: here after referred to as S1), stability problems of two types of shear flows were studied: One is a plane Couette flow bounded in both sides (case I) and another is the same flow but unbounded in one side to connect with a rest fluid (case II). He used analytical solutions expressed by power series and calculated eigenvalues and eigenfunctions with high accuracy. He concluded that, when Froude number is greater than unity, gravity waves are destabilized even by a constant shear flow, and thus they are not related with the existence of inflection point of the basic shear. He also concluded that excited gravity waves can radiate from the shear zone in the case II.

Also Blumen, Drazin, and Billings (1975) had found unstable waves similar to those of S1, but their discussion about the characteristics of the unstable waves had been insufficient. One of the purposes of S1 was to clarify the nature of the unstable mode. Further comparison among S1 and Blumen *et al.* or other studies was presented in S1 and Satomura (1981b) where he used a piecewise-linear flow unbounded in both sides and compared the results with those of Drazin and Davey (1977).

In the previous paper S1, a curious nature of the unstable wave was pointed out, that is, the unstable wave growing in a constant potential vorticity field can not change potential vorticity at all. It means that a change of zonal mean flow, $\partial\bar{u}/\partial t$, does not occur unless zonal mean depth $\bar{h}$ changes. But, when disturbances disappear for some reason, $\bar{h}$ must be constant and, thus, no change of $\bar{u}$ will remain. Then, a question arose whether the unstable waves can permanently change momenta of basic flows. The analysis of S1, however, was a linear theory, and only suggestions for an answer of this question was given.

A purpose of this paper is to investigate the effects of nonlinearity and viscosity upon the unstable waves, and to examine whether perma-

nent redistribution of momentum occurs or not.

A next step of a linear analysis may be a finite amplitude (but weak nonlinear) analysis. But, for the channel model we use, the critical wavenumber which corresponds to the fastest growing mode at the critical Froude number (=2) is infinite. This fact makes the finite amplitude analysis difficult. Moreover, no experiment nor numerical simulation, which guides us into an appropriate hypothesis such as shape assumption, has been performed. In this paper, we will integrate basic equations numerically and present results of integrations.

In the next section, we present shallow water equations as basic equations and describe numerical channel model. A constant shear flow is used as a basic flow in the channel. Thus, the model is the same as the case I of S1. In section 3, results of inviscid run are described at first, and, then, results of viscous run are discussed. Some of the results are the same as those suggested by the linear theory S1 but some of them are not. Summary and conclusions are presented in section 4. A detailed expression of finite-difference scheme is given in appendix A, and a derivation of energy equations is given in appendix B. In appendix C, viscous terms in a shallow water equations are derived.

2. Basic equations and numerical model

We shall consider a plane parallel flow of a shallow water. The model described below is schematically shown in Fig. 1. The fluid is bounded by two vertical walls, assumed to be rigid and to be separated by a distance L_y^* as in the case I of S1. Cartesian co-ordinates are defined, with x^* along the walls and y^* normal to the walls. The corresponding velocity components are u^* and v^*, respectively. The fluid depth is h^* and assumed to be H at rest. By introducing a velocity scale U_0, dimensionless variables are written as

$$(x, y)=(x^*, y^*)/L_y^*\,, \quad t=t^*U_0/L_y^*\,,$$
$$(u, v)=(u^*, v^*)/U_0\,, \quad h=h^*/H\,, \qquad (2.1)$$

where variables without asterisks are dimensionless.

The two dimensionless parameters relevant to the present problem are the Froude number Fr and the Reynolds number Re:

$$F_r=U_0/\sqrt{gH}\,, \quad R_e=U_0L_y^*/\nu\,, \qquad (2.2)$$

where g is the gravity acceleration and ν is the coefficient of kinetic viscosity and these quantities are assumed to be constants. Since it is not a subject of this paper to study whole aspects of high speed flows, we only consider $Fr=5$ for all cases, and $Re=3000$ (viscous case) or infinite (inviscid case).

Then, the dimensionless equations of motion and continuity in a shallow water are

$$\frac{\partial \boldsymbol{V}}{\partial t}+u\frac{\partial \boldsymbol{V}}{\partial x}+v\frac{\partial \boldsymbol{V}}{\partial y}+\frac{1}{F_r^2}\nabla h=\frac{1}{R_e}\boldsymbol{F}\,, \qquad (2.3)$$

$$\frac{\partial h}{\partial t}+\nabla(h\boldsymbol{V})=0\,, \qquad (2.4)$$

where $\boldsymbol{V}$ is the velocity, $\boldsymbol{F}$ is the viscous term and

$$\nabla=\left(\frac{\partial}{\partial x}, \frac{\partial}{\partial y}\right).$$

The channel width, Ly, is unity, and boundary conditions at the walls are

$$v=0 \quad \text{at } y=\pm 1/2 \qquad (2.5a)$$

in the inviscid case, and

$$v=0, \quad u=\pm 1/2 \quad \text{at } y=\pm 1/2 \qquad (2.5b)$$

in the viscous case. In the x direction, the channel length is Lx, and fluid is assumed to continue cyclically.

The initial conditions for time integration are

$$u=y+\delta u\,,$$
$$v=0\,, \qquad (2.6)$$
$$h=1+\delta h\,,$$

where δu and δh are small random perturbations, and are connected with each other by a following relation:

$$q\equiv\frac{\dfrac{\partial v}{\partial x}-\dfrac{\partial u}{\partial y}}{h}=\frac{-1-\dfrac{\partial(\delta u)}{\partial y}}{1+\delta h}=-1\,. \qquad (2.7)$$

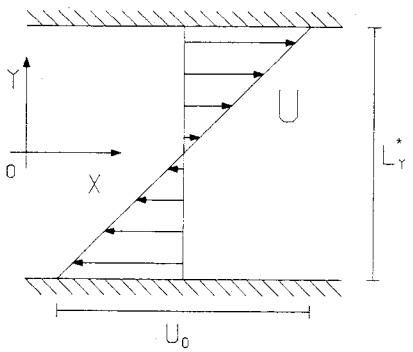

Fig. 1 The model of numerical integration. Dimensionless width is 1 and dimensionless basic flow varies from 0 to 1. Surface elevates normally to the paper.

Above relation is set to bring the numerical model close to the analytical model of S1, because, in the linear theory, no potential vorticity is added by perturbations superposed on a constant shear flow (see equations (5.3) and (5.4) of S1).

Finite-difference scheme for the space coordinates of (2.3) and (2.4) follows Arakawa and Lamb (1981). It conserves total mass, energy, and potential enstrophy $q^2/2h$. Some of the reasons why we choose this complicated scheme are that zero potential vorticity of the disturbance is an important characteristic, and, thus, there is a risk that non-physical change of q by a finite-difference approximation cause a serious error. The explicit form of the finite-difference scheme is shown in appendix A.

The scheme of time difference is the forward difference for the viscous term and the leap-frog scheme for the other terms.

The number of grid points in the x and the y directions are 64×20 in the inviscid case, and 32×10 in the viscous case. Grid intervals are $d=\Delta x=\Delta y=0.05$ and 0.1 in the inviscid and viscous case, respectively. Thus, the domain of the present numerical integration is that $Lx=3.25$ and $Ly=1.0$ in the inviscid case, and that $Lx=3.3$ and $Ly=1.0$ in the viscous case in dimensionless unit. These values of Lx's are about twice as long as the wavelength of the most rapidly growing wave for $Fr=5$ in S1. So far as parameters used in this paper, errors by the finite-difference approximations are not serious, and, thus, we suppose that the numerical solutions indicate characteristics of the true solutions.

3. Results

In this section, results and discussions of inviscid run are described in the first subsection, and those of viscous run are presented in 3.2. In both runs, the Froude number is fixed to five, and only the Reynolds numbers are different between them.

In the following discussions, $\overline{(\ )}$ denotes zonally averaged quantity and $(\ )'=(\ )-\overline{(\ )}$ is the deviation from it.

3.1 *Inviscid case ($Re\to\infty$)*

When Re tends to be infinity, growth rates and structures of the numerical solutions should be the same, at least its initial stage, as those of the linear theory. Fig. 2 shows time variation of potential energy of each Fourier component.

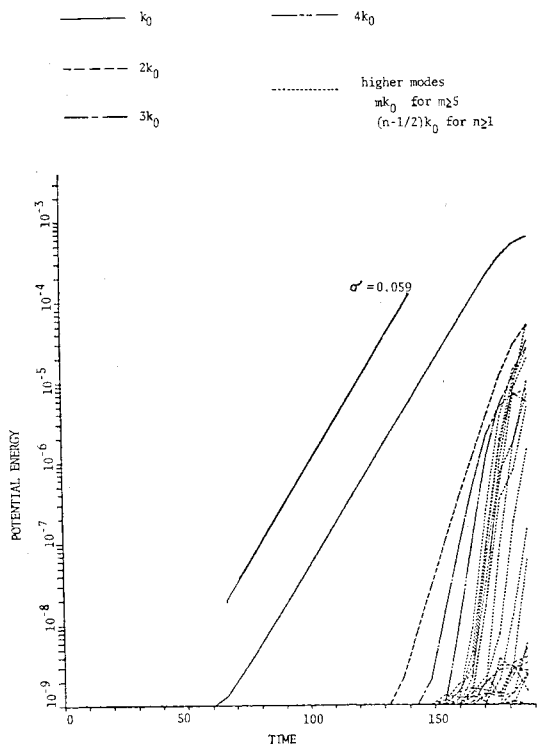

Fig. 2 Time variation of potential energy for each Fourier component in the inviscid case. Thick solid line indicates a growth rate $\sigma=0.059$.

From this figure, it is found that the growth rate of the first appeared mode is 0.059, and is in good agreement with the theoretical value 0.0585. Of course, the wavenumber of the first appeared mode, $k_0=3.8$, is the same as that indicated by the theory.

Since the Froude number is greater than 2, the time when nonlinear effects become dominant is also interesting. Fig. 2 indicates that higher modes $k=2k_0, 3k_0, \ldots$, are excited by the nonlinearity and their amplitudes can be seen only for the later stage of the run ($t>150$). Thus, the linear stability analysis retains its usefulness even for $Fr=5$. When we numerically integrate the equations (2.3) and (2.4) to a little further beyond $t\approx190$, the result has no longer a physical meaning due to the errors which increase as the amplitudes of the higher harmonics of the order of grid sizes become large.

The structure of the disturbance at $t=143.165$ is shown in Fig. 3. It is a typical structure in an early stage of the development of the disturbance, and it also agrees well with theoretically composed one: phases of troughs and ridges tilt

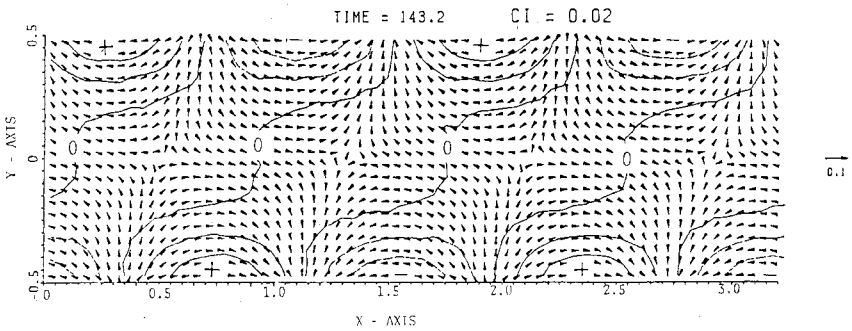

Fig. 3 Structure of disturbance at $t=143.165$ in the inviscid case. Arrows denote velocity (u',v') and solid lines are contours of $h=\bar{h}+h'$. Contour interval is 0.02.

to the positive x direction with increasing y, and, the maxima of divergence and convergence are at the left side (the smaller x side) of the troughs and of the ridges respectively near the wall at $y=1/2$, and vice versa near the wall at $y=-1/2$. The total pattern is similar to the gravity waves in a channel.

Fig. 4 shows a typical x-variation of the disturbed depth, h', at $y=0.475$ for three stages. In the early stage ($t=143.165$), h' varies sinusoidally and symmetrically with x. But, as the amplitude increases, asymmetry appears in an intermediate stage ($t=165.165$), and a shape similar to a shock wave is formed in a strong-nonlinear stage ($t=187.165$). At this time, perturbation Froude number F_{rp}, which is defined as $F_{rp}=U_p/\sqrt{g\bar{H}}$ by introducing characteristic velocity of wave part U_p, is nearly equal to unity. Inspecting the asymmetry of h' in Fig. 4 closely, we notice that $|\partial h/\partial x|$ is larger in the left side (the smaller x side) of peaks than the right side (the larger x side). It suggests us that, on the analogy of formation of shock waves, waves near the wall at $y=1/2$ are propagating to the negative x direction relative to the flow. Near the wall at $y=-1/2$, on the other hand, waves are supposed to be propagating

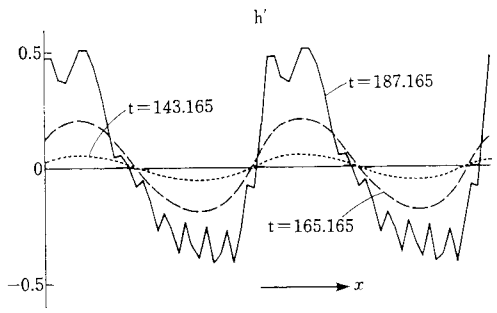

Fig. 4 Disturbance depth h' at $y=0.475$ for three values of t in the inviscid case.

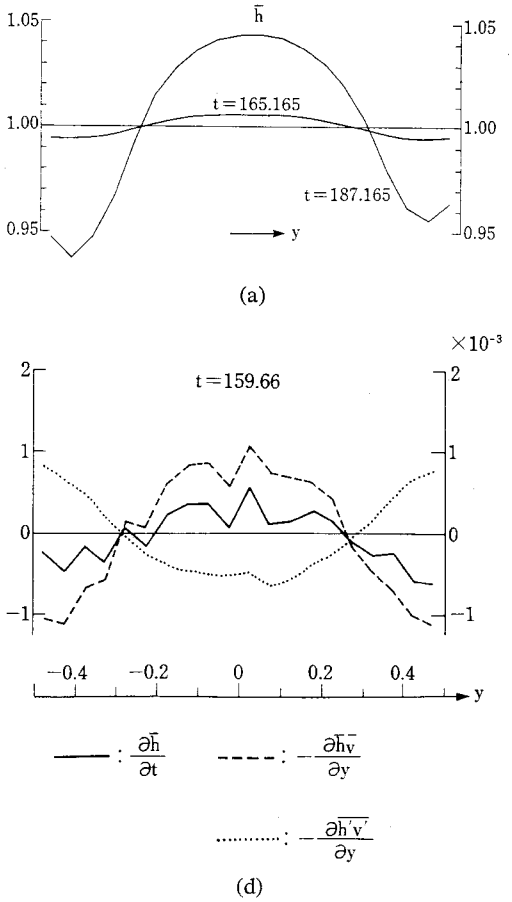

Fig. 5 (a) Zonal mean depth $\bar{h}$ for $t=165.165$ and $t=187.165$ and (b) values of terms in the equation of $\bar{h}$ for $t=159.66$ in the inviscid case.

to the positive x direction. What are mentioned above confirm the discussion of S1 about Figs. 3(a) and 4(a) of that paper (p. 157~158), and are consistent with the conclusion of S1 that the unstable waves are destabilized gravity waves in a channel.

Fig. 5(a) depicts zonal mean depth $\bar{h}$ at $t=165.165$ and $t=187.165$. We see that zonal mean mass concentrates on the center of the channel more and more with time. To find the term which produces this concentration, let us examine the equation of $\bar{h}$. It is written from (2.4) as

$$\frac{\partial \bar{h}}{\partial t}+\frac{\partial}{\partial y}\bar{h}\bar{v}+\frac{\partial}{\partial y}\overline{h'v'}=0\,, \tag{3.1}$$

At the initial time $v=0$ and $\bar{h}=1$, thus the first term in the left-hand side of (3.1) should be balanced with the last term. The last term can be evaluated by the eigenfunctions presented in S1, and is positive near the center of the channel and negative near the walls. Thus, the linear theory predicts that $\bar{h}$ should become shallow with time near the center and deep near the walls. But, what happens in the numerical integration is opposite. An example of values of terms of (3.1) are shown in Fig. 5(b) for the numerical solution at $t=159.66$. (Small scale disturbances may be hardly related with physical phenomena because the truncation error is up to 10^{-4}.) We find that the last term of (3.1) is the same sign as the linear analysis, but the second term, neglected in the linear analysis(*), controls the time change of $\bar{h}$. This nature does not change through the numerical integration except at the earliest time.

Fig. 6 shows time variation of momentum averaged in the half area (abbreviated to MHA), which is defined as

$$\langle\overline{hu}\rangle=\langle\bar{h}\bar{u}+\overline{h'u'}\rangle=2\int_0^{1/2}\overline{hu}\,dy\,. \tag{3.2}$$

From the equation (2.3), we obtain a following equation for $\langle\overline{hu}\rangle$ as

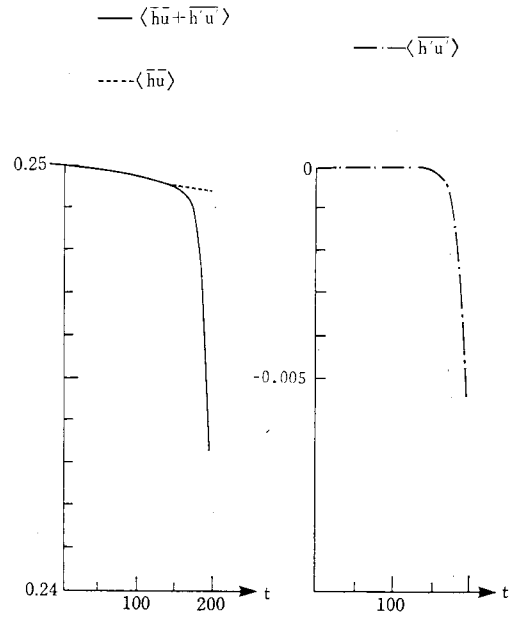

Fig. 6 Time variation of the half momentum MHA in the inviscid case.

$$\frac{\partial}{\partial t}\langle\bar{h}\bar{u}+\overline{h'u'}\rangle=2[\overline{huv}]_{y=0}\,. \tag{3.3}$$

Thus MHA is changed by the momentum flux from the 'upper' half zone ($0<y<1/2$) to the 'lower' half zone ($-1/2<y<0$). From Fig. 6, the 'upper' momentum decreases with time, *i.e.*, momentum is transported to the 'lower' half, and redistributed. It is also found that most part of the decrease of MHA is $\langle\overline{h'u'}\rangle$. These properties of momentum change are consistent with those in S1 and they also give a hope for a permanent change of momentum by the unstable waves under viscous effects.

The energy balance at $t=165.165$ is shown in Fig. 7. A detailed derivation of the energy equations and definitions of symbols are given in appendix B. This four box diagram indicates that the disturbance kinetic energy K' receives energy through the $[\bar{K}K']$ transformation. The disturbance potential energy P' receives energy through $[K'P']$ and returns only a little energy to the mean kinetic energy $\bar{K}$. It is also found from Fig. 7 that the total disturbance energy $K'+P'=33\times10^{-5}$ and equals to the absolute value of the additional part of the mean kinetic energy K_a. The relation,

$$K'+P'+K_a=0\,, \tag{3.4}$$

was derived in S1 under the condition of the

(*) If we assume

$$\frac{\partial \bar{h}\bar{v}}{\partial t}\propto\bar{h}\left(\overline{u'\frac{\partial v'}{\partial x}}+\overline{v'\frac{\partial v'}{\partial y}}\right),$$

the second term of (3.1) can be evaluated and is consistent with the numerical results shown in figure 5(b). We cannot evaluate, however, $\bar{h}\bar{v}$ directly, but only $\partial\bar{h}\bar{v}/\partial t$. And, $\partial\bar{h}\bar{v}/\partial t$ will affects only the higher order trend $\partial^2\bar{h}/\partial t^2$. Thus, it seems appropriate to neglect the second term of (3.1) in the linear theory.

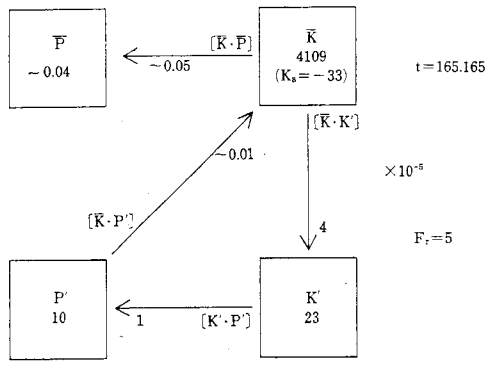

Fig. 7 Four-box energy diagram at $t=165.165$ in the inviscid case.

constant shear flow, and it means that K_a plays an important role in the energy budget. The fact that (3.4) is satisfied in good accuracy in numerical integration means that the total nature of the finite-amplitude numerical solution closely resembles the characteristics of the eigenfunction in S1. A projection of this interesting property to the momentum budget is the fact that $|\langle\overline{h'u'}\rangle| \gg |\langle\bar{h}\bar{u}\rangle - 0.25|$.

3.2 Viscous case ($Re=3000$)

In this subsection, results of viscous run for $Re=3000$ are presented. Before the results are shown, it should be took notice that the viscous term $\boldsymbol{F}$ is rather unusual, and it is expressed as

$$\boldsymbol{F}=(F_x, F_y), \tag{3.5}$$

where

$$F_x=\frac{1}{h}\left[\frac{\partial}{\partial x}\left(2h\frac{\partial u}{\partial x}\right)+\frac{\partial}{\partial y}\left\{h\left(\frac{\partial u}{\partial y}+\frac{\partial v}{\partial x}\right)\right\}\right], \tag{3.6}$$

$$F_y=\frac{1}{h}\left[\frac{\partial}{\partial x}\left\{h\left(\frac{\partial u}{\partial y}+\frac{\partial v}{\partial x}\right)\right\}+\frac{\partial}{\partial y}\left(2h\frac{\partial v}{\partial y}\right)\right]. \tag{3.7}$$

These forms include effects of the free surface on stress tensor. Detailed derivation of (3.6) and (3.7) is given in appendix C.

Fig. 8(a) shows time variation of total energy of disturbances $K'+P'$ and Fig. 8(b) shows time variation of potential energy of each wavenumber. Nature of both time variations for $t>850$ depends strongly on both the grid intervals of space difference and the definition of the potential vorticity at the walls. Thus, we will not discuss the results for $t>850$, although numerical integration can be stably extended for a long time.

From these figures, following aspects of time variations are seen:

(a) At first, disturbance grows exponentially and its growth rate $\sigma\approx 0.036$ and wavenumber $k_0=3.8$. These values are in good agreement with the values estimated by the linear theory ($\sigma_l\approx 0.032$(*), $k_0=3.8$, respectively).

(b) Higher harmonics with wavenumbers $2k_0$, $3k_0$, $4k_0, \ldots$, are excited one after another by nonlinear effects, and viscosity stops growing of disturbances. ($240\lesssim t\lesssim 300$)

(c) Energy of disturbances decreases and reaches a quasi-steady state. ($300\lesssim t\lesssim 500$)

(d) Modes whose wavenumbers are $(n-1/2)k_0$ grow with oscillation, although disturbances with wavenumbers nk_0, where $n=0, \pm 1, \pm 2, \ldots$, are still in quasi-steady state. ($500\lesssim t\lesssim 700$)

(e) Amplitudes of $(n-1/2)k_0$ modes become large and oscillations both of the potential energy of nk_0 modes and of the total disturbance energy become evident. ($700\lesssim t$)

The stages (a)~(c) are rather ordinary characteristics. But, in the stages (d) and (e), an interesting feature of growing oscillation appears. Fig. 9 is a close-up of Fig. 8(b) for $469\lesssim t\lesssim 522$. It shows that the period of oscillating mode $T\approx 9$ and the phase of $k_0/2$ mode is earlier than that of $3/2k_0$ mode about $\pi/2$. It also shows that the amplitude of h^2 or $k_0/2$ mode is about 1.5 times as large as that of $3/2k_0$ mode. On the other hand, no oscillation is looked in nk_0 mode from this figure. But, from a much larger magnified figure (not shown), it is found that, at least, the potential energy of k_0 mode is oscillating in the same order of the amplitude as that of $k_0/2$ mode and is out phase with $k_0/2$ mode.

Then, why do $k_0/2$ and $3/2k_0$ modes grow? And, why does their potential energy oscillate with that period?

In order to answer above questions, let us examine a linear stability of the quasi-steady state.

As the first step of the analysis, divide the physical quantities into two parts as

(*) The growth rate σ_l is estimated by following equation

$$\sigma_l=\sigma_i-\frac{k^2+l^2}{Re},$$

where σ_i is the growth rate in the inviscid linear theory, k and l are the wavenumbers in the x and y direction respectively. Here, we assumed that eigenfunction is the same as that of the inviscid linear theory and that viscous terms are expressed by the usual Laplacian form.

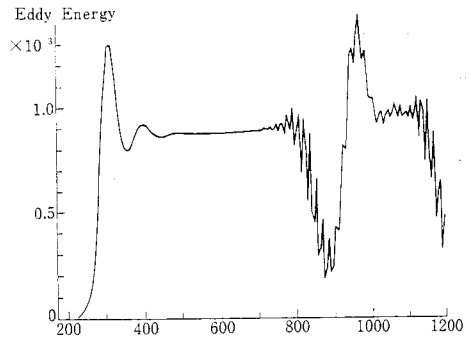

(a)

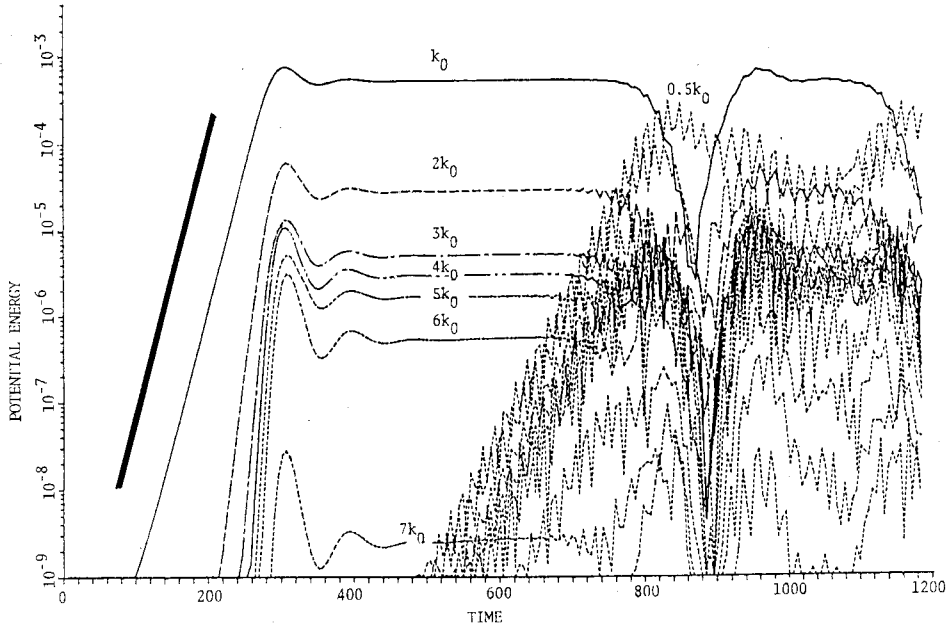

(b)

Fig. 8 Time variation of (a) total perturbation energy and (b) potential energy of each Fourier component for $Re=3000$. Thick solid line in (b) indicates a growth rate $\sigma=0.036$.

$$V=V^{(0)}+V^{(1)}, \quad h=h^{(0)}+h^{(1)}, \tag{3.8}$$

where superscripts (0) and (1) indicate a basic state and infinitesimal perturbations, respectively. The basic state is assumed to be composed of three parts as

$$V^{(0)}=V_0+V_1e^{ik_0x}+\text{conjugate term},$$
$$h^{(0)}=h_0+h_1e^{ik_0x}+\text{conjugate term}, \tag{3.9}$$

where subscripts 0 and 1 indicate the zonal part and the wavy part, respectively.

We also assume that perturbation quantities are written as

$$V^{(1)}=(V_{1/2,(+)}e^{ik_0x/2}+V_{3/2,(+)}e^{3ik_0x/2})e^{i\omega t}+(V_{1/2,(-)}e^{ik_0x/2}+V_{3/2,(-)}e^{3ik_0/2})e^{-i\omega t}+\text{conjugate terms},$$
$$h^{(1)}=(h_{1/2,(+)}e^{ik_0x/2}+h_{3/2,(+)}e^{3ik_0x/2})e^{i\omega t}+(h_{1/2,(-)}e^{ik_0x/2}+h_{3/2,(-)}e^{3ik_0x/2})e^{-i\omega t}+\text{conjugate terms}. \tag{3.10}$$

where subscripts $1/2$ and $3/2$ indicate $k_0/2$ mode and $3k_0/2$ mode respectively, and subscripts $(+)$ and $(-)$ indicate signs of frequencies. This assumption is appropriate if Fourier expansion of perturbation quantities converges rapidly. It

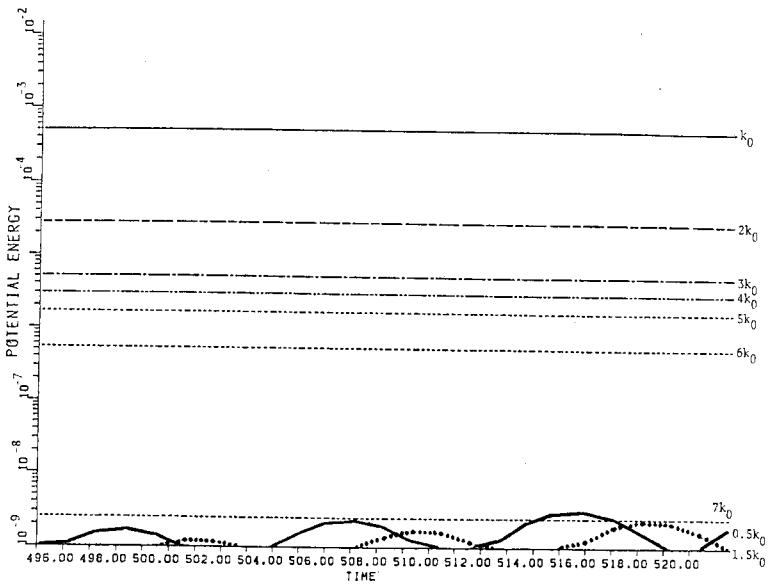

Fig. 9 Close-up of Fig. 8(b) for $496 \leqq t \leqq 522$.

would be also suitable if eigenvalues and eigenfunctions do not change significantly by including higher modes such as $\pm 5k_0/2$. The variation of sub-harmonics, $\pm k_0/2$, are examined by removing $\pm 3k_0/2$ modes instead of including higher modes, and it is found that they change only a little. Thus, the closure assumptions (3.10) and (3.11) is not a poor approximation.

Now, using (3.8) (3.11), perturbation equations are obtained from (A.1)(*) as

$$\pm i\omega V_{1/2,\substack{(+)\\(-)}} + q_0\boldsymbol{k}\times\hat{V}_{1/2,\substack{(+)\\(-)}} + q_1\boldsymbol{k}\times\hat{V}^{\dagger}{}_{1/2,\substack{(-)\\(+)}} + q_1{}^{\dagger}\boldsymbol{k}\times\hat{V}_{3/2,\substack{(+)\\(-)}} + q_{1/2,\substack{(+)\\(-)}}\boldsymbol{k}\times\hat{V}_0 + q^{\dagger}{}_{1/2,\substack{(-)\\(+)}}\boldsymbol{k}\times\hat{V}_1 + q_{3/2,\substack{(+)\\(-)}}\boldsymbol{k}\times\hat{V}_1{}^{\dagger} + \nabla\left(V_0V_{1/2,\substack{(+)\\(-)}} + V_1V^{\dagger}{}_{1/2,\substack{(-)\\(+)}} + V_1{}^{\dagger}V_{3/2,\substack{(+)\\(-)}} + \frac{1}{F_r{}^2}h_{1/2,\substack{(+)\\(-)}}\right) = \frac{1}{R_e}\left\{\frac{\partial^2}{\partial y^2} - \left(\frac{k_0}{2}\right)^2\right\}V_{1/2,\substack{(+)\\(-)}}, \tag{3.12}$$

$$\pm i\omega h_{1/2,\substack{(+)\\(-)}} + \frac{ik_0}{2}\hat{u}_{1/2,\substack{(+)\\(-)}} + \frac{\hat{\partial}}{\partial y}\hat{v}_{1/2,\substack{(+)\\(-)}} = 0, \tag{3.13}$$

$$\pm i\omega V_{3/2,\substack{(+)\\(-)}} + q_0\boldsymbol{k}\times\hat{V}_{3/2,\substack{(+)\\(-)}} + q_1\boldsymbol{k}\times\hat{V}_{1/2,\substack{(+)\\(-)}} + q_{3/2,\substack{(+)\\(-)}}\boldsymbol{k}\times\hat{V}_0 + q_{1/2,\substack{(+)\\(-)}}\boldsymbol{k}\times\hat{V}_1 + \nabla\left(V_0V_{3/2,\substack{(+)\\(-)}} + V_1V_{1/2,\substack{(+)\\(-)}} + \frac{1}{F_r{}^2}h_{3/2,\substack{(+)\\(-)}}\right) = \frac{1}{R_e}\left\{\frac{\partial^2}{\partial y^2} - \left(\frac{3k_0}{2}\right)^2\right\}V_{3/2,\substack{(+)\\(-)}} \tag{3.14}$$

$$\pm i\omega h_{3/2,\substack{(+)\\(-)}} + \frac{3ik_0}{2}\hat{u}_{3/2,\substack{(+)\\(-)}} + \frac{\hat{\partial}}{\partial y}\hat{v}_{3/2,\substack{(+)\\(-)}} = 0, \tag{3.15}$$

where a dagger denotes a complex conjugate, $\boldsymbol{k}$ is a vertical unit vector,

$$\hat{V}_0 = (hV)_0, \tag{3.16}$$

$$\hat{V}_1 = (hV)_1, \tag{3.17}$$

$$\hat{V}_{1/2,\substack{(+)\\(-)}} = h_0V_{1/2,\substack{(+)\\(-)}} + h_1V^{\dagger}{}_{1/2,\substack{(-)\\(+)}} + h_1{}^{\dagger}V_{3/2,\substack{(+)\\(-)}} + h_{1/2,\substack{(+)\\(-)}}V_0 + h^{\dagger}{}_{1/2,\substack{(-)\\(+)}}V_1 + h_{3/2,\substack{(+)\\(-)}}V_1{}^{\dagger}, \tag{3.18}$$

$$\hat{V}_{3/2,\substack{(+)\\(-)}} = h_0V_{3/2,\substack{(+)\\(-)}} + h_1V_{1/2,\substack{(+)\\(-)}} + h_{3/2,\substack{(+)\\(-)}}V_0 + h_{1/2,\substack{(+)\\(-)}}V_1, \tag{3.19}$$

$$q_{1/2,\substack{(+)\\(-)}} = \frac{1}{h_0}\left[\frac{ik_0}{2}v_{1/2,\substack{(+)\\(-)}} - \frac{\hat{\partial}}{\partial y}u_{1/2,\substack{(+)\\(-)}} - \frac{1}{h_0}\left\{h_1\left(\frac{ik_0}{2}v_{1/2,\substack{(-)\\(+)}} - \frac{\hat{\partial}}{\partial y}u_{1/2,\substack{(-)\\(+)}}\right)^{\dagger}\right.\right.$$

(*) The reason why (A.1) is used is that we will use a finite-difference scheme instead of the differentiation with y, and that it is easier to make an energy conserving scheme from (A.1) than from (2.3).

$$+h_1^{\dagger}\left(\frac{3ik_0}{2}v_{3/2,\substack{(+)\\(-)}}-\frac{\partial}{\partial y}u_{3/2,\substack{(+)\\(-)}}\right)-\frac{\partial u_0}{\partial y}h_{1/2,\substack{(-)\\(-)}}\Bigg\}-\frac{2}{h_0^2}\frac{\partial u_0}{\partial y}\times(h_1h^{\dagger}{}_{1/2,\substack{(+)\\(-)}}+h_1^{\dagger}h_{3/2,\substack{(+)\\(-)}})\Bigg], \tag{3.20}$$

$$q_{3/2,\substack{(+)\\(-)}}=\frac{1}{h_0}\left[\frac{3ik_0}{2}v_{3/2,\substack{(+)\\(-)}}-\frac{\partial}{\partial y}u_{3/2,\substack{(+)\\(-)}}\right.$$
$$-\frac{1}{h_0}\left\{h_1\left(\frac{ik_0}{2}v_{1/2,\substack{(+)\\(-)}}-\frac{\partial}{\partial y}u_{1/2,\substack{(+)\\(-)}}\right)\right.$$
$$\left.\left.-\frac{\partial u_0}{\partial y}h_{3/2,\substack{(+)\\(-)}}\right\}-\frac{2}{h_0^2}\frac{\partial u_0}{\partial y}h_1h_{1/2,\substack{(+)\\(-)}}\right]. \tag{3.21}$$

In equations (3.12)~(3.17), $\hat{V}_0$, $\hat{V}_1$, q_0, and q_1 are directly calculated from the grid data by Fourier transformation. In equations (3.20) and (3.21), square terms of the wavy parts of the basic state are neglected, because the wavy parts are as one order small as the zonal mean parts.

By using finite-difference approximation to the differentiations with y, and by using the boundary conditions for the perturbations

$$V_{1/2,\substack{(+)\\(-)}}=V_{3/2,\substack{(+)\\(-)}}=0 \qquad \text{at } y=\pm 1/2, \tag{3.22}$$

equations (3.12) (3.15) can be written formally as

$$\boldsymbol{Ab}=\omega\boldsymbol{b}, \tag{3.23}$$

where $\boldsymbol{b}$ is the eigenvector of A to be determined and it describes perturbation field, and A is the coefficient matrix of finite-difference equations. Then, ω and $\boldsymbol{b}$ can be obtained as a numerical solution of the eigenvalue problem (3.23), and the results are shown in Table I and Figs. 10 and 11.

Table 1 Frequency of oscillating modes. Frequency of energy is twice as large as these values

Wavenumber	Numerical integration	Stability analysis
$k_0/2$	$0.36+0.018i$	$0.41+0.006i$
$3k_0/2$	$0.36+0.018i$	

As seen from Table I, the difference between the eigenvalue and the frequencies found by the numerical integration is small for the real part. On the other hand, the imaginary parts of the frequencies of numerical integration are three times as large as that of the eigenvalue, but disagreement between them is supposed to be not so serious that we must seek another cause of the growing oscillation.

It is worth noting that the real parts of the phase velocities of the $1/2k_0$ mode ($=\pm 0.19$

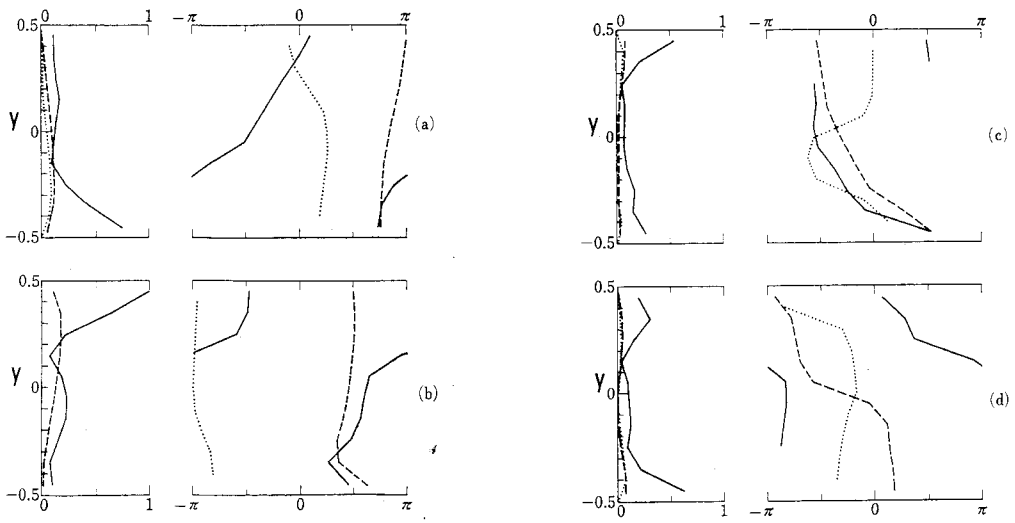

Fig. 10 Amplitude (left half) and phase (right half) of eigenfunction for (a) $\exp\{i(k_0/2-\omega t)\}$ mode, (b) $\exp\{i(k_0/2+\omega t)\}$ mode, (c) $\exp\{i(3k_0/2-\omega t)\}$ mode, and (d) $\exp\{i(3k_0/2+\omega t)\}$ mode. Solid curve is the eigenfunction of $h^{(1)}$, dashed curve is that of $u^{(1)}$, and dotted curve is that of $v^{(1)}$. Phases indicate the maximum values of each eigenfunction.

from the numerical results and ± 0.22 from the stability analysis) are almost equal to those of the linear inviscid theory, ± 0.225 (see Fig. 3(a) of S1). This fact suggests that a mechanism similar to a resonance is acting, *i.e.*, neutral eigen-modes are likely destabilized resonantly by energy supply from the basic state, especially from k_0 mode.

Amplitudes(*) and phases of eigenfunctions are shown in Fig. 10. The relation between the location of the maximum amplitude and sign of the phase velocity of $k_0/2$ mode agrees with the discussion of S1 (p. 156~157), *i.e.*, the mode which has a phase velocity faster than the y-averaged zonal flow, which is 0.5 in S1 and 0 in this paper, has a large amplitude near the wall at $y=-1/2$ and vice versa. This agreement supports the suggestion of the resonant destabilization described little earlier.

For $3/2k_0$ modes, the relation between the amplitude and the phase velocity is reversed. It might be explained that these modes correspond to the destabilized neutral modes which exist along neutral lines through (1.1) mode and (1.2) mode or the line through (1.1) mode and (2.1) mode of S1 (see Fig. 3(a) of S1). But, such correspondence to the neutral modes of S1 is worse than $k_0/2$ modes.

Fig. 11 depicts time variation of the potential energy calculated by eigenfunctions. The reason why the potential energy oscillates is as follows: There are two waves in each wavenumber and one of them propagates to the positive x direction and another wave propagates to the opposite direction (see equation (3.11)). For simplicity, the perturbation depth of a wavenumber k is re-written as

$$h=h_{1(y)}e^{i(kx-\omega t)}+h^{\dagger}{}_{1(y)}e^{-i(kx-\omega t)} +h_{2(y)}e^{i(kx+\omega t)}+h^{\dagger}{}_{2(y)}e^{-i(kx+\omega t)}, \quad (3.24)$$

where h_1 and h_2 are the amplitudes. Then, the perturbation potential energy P.E. of the wavenumber k becomes

$$P.E.\propto\int_{-1/2}^{1/2}\overline{|h|^2}dy\propto\int_{-1/2}^{1/2}(|h_1|^2+|h_2|^2)dy +2\int_{-1/2}^{1/2}\mathrm{Real}(h_1h_2^{\dagger}e^{2i\omega t})dy, \quad (3.25)$$

where Real ( ) indicates real part. The second integration of the right-hand side of (3.25) causes the oscillation with a half period of the original waves. Physically, this term comes from the fact that two waves are in-phase and out-phase periodically owing to the propagation in the opposite direction with each other. If $h_1=h_2$, these two waves form a standing wave. Of course, the sum of the potential energy and the kinetic energy of the wavenumber should be a constant if the waves are linear and neutral. Hence, the oscillation of P.E. is an apparent one, in this sense. But, waves in our case are growing modes and the perturbation total energy oscillates due to the oscillations of u and v, *i.e*, the oscillation of the Reynolds stress. This oscillation of the disturbance total energy becomes obvious for $t\gtrsim 700$ in Fig. 8.

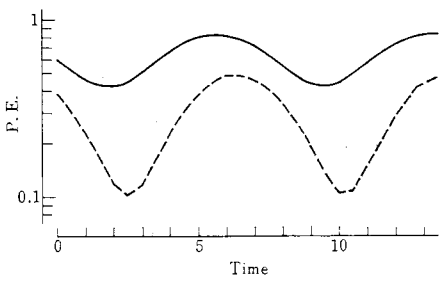

Fig. 11 Time variation of potential energy of the eigenfunction. Solid curve is $k_0/2$ mode and dashed curve is $3k_0/2$ mode. Absolute value of the potential energy is arbitrarily.

As shown in Fig. 11, the phase of the potential energy oscillation of $3/2k_0$ mode lags behind that of $k_0/2$ mode, and it is the same tendency as the results of the numerical integration. The value of the phase lag is, however, about $\pi/4$ and is about a half of the numerical results. The ratio of potential energy of $3/2k_0$ mode to that of the $k_0/2$ mode is also smaller than that of the numerical results. But, we may regard that these differences are not crucial and that these disagreements can be reduced by including the higher harmonics both $2k_0$, $3k_0$, . . ., in the basic state, and $5/2k_0$, $7/2k_0$, . . ., in the perturbation structure.

From the above discussion we interpret that the oscillations shown in Figs. 8 and 9 are produced by the oppositely propagating waves destabilized by both the zonal shear flow and the steady disturbance of the wavenumber k_0.

The structure of the disturbance at $t=495$ is shown in Fig. 12. It is the structure in the quasi-steady state where the viscosity plays an im-

(*) There is a small difference of the maximum amplitudes between $k_0/2$ modes and also between $3k_0/2$ modes. The cause is an asymmetry of the basic field.

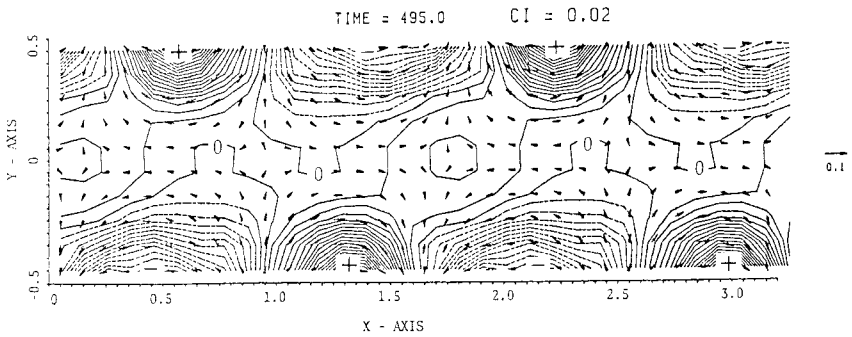

Fig. 12 Structure of disturbance at $t=495$ for $Re=3000$. Arrows denote velocity (u', v') and solid curves are contours of $h=\bar{h}+h'$. Contour interval is 0.02.

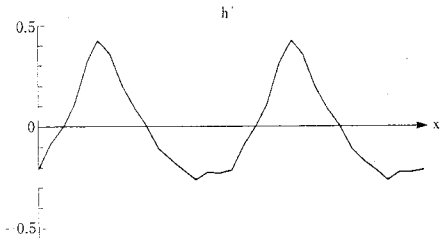

Fig. 13 Disturbance depth h' at $y=0.45$ for $Re=3000$ at $t=495$.

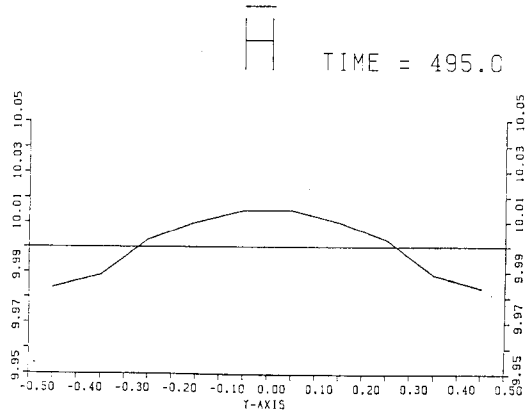

Fig. 14 Zonal mean depth h for $Re=3000$ at t=495. The ordinate is magnified by ten times.

portant role, but it is still similar to the structure of the linear theory S1. The asymmetry of the maxima and minima of depth near the walls are emphasized by a variation of h with y, which is shown in Fig. 14. (Note that a contour indicates a total depth $\bar{h}+h'$).

Fig. 13 shows the disturbance depth h' at $y=0.45$. It is seen that it differs from a sinusoidal variation, but, due to the viscosity, the amplitudes of higher wavenumbers are not large. Compared with the inviscid results at $t=187.165$ (see Fig. 4), the shape similar to a shock wave is disappear and symmetry between right and left sides of ridges is held better.

The zonal mean depth $\bar{h}$ at $t=495$ is shown in Fig. 14. We see that $\bar{h}$ has its maximum near the center of the channel and the minima near the walls. It is the same as the results of the inviscid run and is also an opposite tendency to the supposition from the linear theory. The reason of this opposite tendency is the same as that in the inviscid run. Of course, the mean depth is also quasi-steady about this time and oscillates when oscillation amplitudes of disturbances become large ($t\gtrsim 750$).

Fig. 15 depicts time variation of MHA. Decrease of MHA is about 2% in the quasi-steady state and the contributions $\langle\bar{h}\bar{u}\rangle$ and $\langle\overline{h'u'}\rangle$ are almost the same. Thus, we conclude that, in a viscous fluid, unstable gravity waves

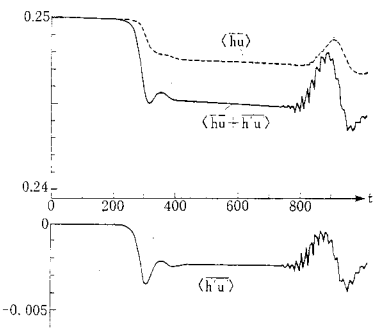

Fig. 15 Time variation of the half momentum MHA for $Re=3000$.

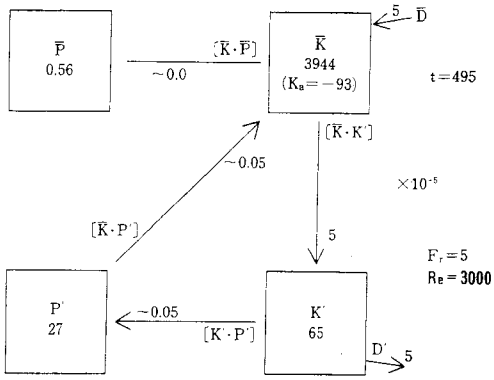

Fig. 16 Four-box energy diagram at t=495 for Re=3000.

can cause a permanent change of the momentum in spite of the uniform vorticity of the initial basic field. For $t \gtrsim 750$, the oscillation appears in $\langle \bar{h}\bar{u}+\overline{h'u'} \rangle$, but the amplitude of the oscillation of $\langle \bar{h}\bar{u} \rangle$ is much smaller than that of $\langle \overline{h'u'} \rangle$. It indicates that the energy conversions among oscillating modes are almost closed within the disturbance energy K', P', and the additional mean kinetic energy K_a. It also indicates that the relation (3.4) is satisfied.

The wavenumber at which the energy is mostly dissipated is estimated (not shown) and is k_0 as expected. This fact confirms the above description about the momentum budget. They are consistent with the energy budget described below.

The energy balance in the quasi-steady state is shown in Fig. 16. This four box diagram shows that the directions of the energy transformations are the same as those of the inviscid run. Because this diagram is depicted for the quasi-steady state, the in-flow and the out-flow of the each potential energy $\bar{P}$ and P' cancel out, and the transformation $[\bar{K}K']=5\times10^{-5}$ is the same as the energy dissipation rate of the disturbances. From this figure, it is also seen that the energy is supplied to $\bar{K}$ by the mean viscous force $\bar{D}$ and is dissipated by the disturbance viscous force D' acting on K'. This fact confirms the statement that disturbances permanently mixed the zonal mean momentum.

4. Summary and conclusions

In the present study, we have numerically investigated time development of unstable gravity waves in a shallow water with and without viscosity. The results are summarized as follows: In the inviscid case, the disturbance which has the structure quite similar to that of the linear unstable wave grows exponentially at first. Its growth rate is the same as that of S1. The larger the amplitude became, the more significant the nonlinear effect became. Finally, the structure of the disturbance formed a shape similar to a shock wave, and the numerical integration was broken down. This shock wave shape of the last stage of the numerical run confirms the discussion of S1 about the dispersion diagram (Fig. 3(a) or 4(a)).

The momentum mixing, which was one of the motivations of the present study, was occurred at least temporarily in the inviscid case. The energy budget showed that only the mean kinetic energy $\bar{K}$ is the origin of all other energy, and the transformations $[\bar{K}K']$, $[\bar{K}\bar{P}]$, and $[K'P']$ are all positive.

In the viscous run, on the other hand, the same disturbance as that in the inviscid run grew exponentially, and reached a quasi-steady state. In this quasi-steady state, the momentum of the half area, MHA, was reduced by 2%. It suggests us that the unstable gravity waves can mix the momentum permanently.

The quasi-steady state was unstable for $(n-1/2)k_0$ mode. The unstable modes had a frequency $\omega \approx 0.36$ and growth rate $\sigma \approx 0.018$. There were two phase velocities of opposite signs for each wavenumber, and the energy of each wavenumber oscillates with a frequency 2ω. To explain these unstable waves and oscillations, a linear analysis in which the basic state was composed of two parts, the zonal flow and the k_0 mode, was examined. Obtained eigenvalues and eigenfunctions agreed with the results of the numerical integration.

The energy balance in the quasi-steady state showed that the viscous effect near the walls creates the mean kinetic energy $\bar{K}$, most part of the created energy is transformed to the disturbance kinetic energy K', and, then, dissipated by the viscosity acting on the disturbances.

If the channel is much more longer than that used in this paper, the most unstable wave growing in the quasi-steady state may not be $(n-1/2)k_0$ mode but the side-band mode $(n\pm\alpha)k_0$ where α is a real number. Indeed, by an stability analysis for the side band modes, we find that side band modes of $\pm0.4k_0$, $\pm(1\pm0.4)k_0$ are the most unstable modes in the quasi-steady state.

Their growth rate is seven times as large as the sub-harmonics. But, adding to the fact that the wavelengths are similar to those of the sub-harmonics, the real part of the eigenvalue is almost the same as that of the sub-harmonics. Thus, results of a long channel model will not change quantitatively.

As mentioned in the previous paper S1, unstable gravity waves possibly play a certain role in actual geophysical fluids, because Fr is able to exceed unity easily for internal waves in stratified fluids. Although wave energy is concentrated near the walls in a channel model, Blumen, Drazin, and Billings (1975) and Satomura (1981b) showed that gravity waves can grow without walls and radiate to infinity. In many cases, growth rates of the present instability may be smaller than those of barotropic or baroclinic instability, but the present mechanism has a point of advantage that a zonal flow becomes unstable with no inflection point of the flow, no rotation of planets, and no temperature variation of the basic field. Thus, if an excitation of disturbances is found by observations in a barotropically and baroclinically stable area, the present mechanism will be a strong candidate for the excitation.

Present mechanism is also one of the candidates for mechanisms to excite gravity waves whose wavelength is hundreds of kilometers and which are observed in the middle atmosphere (see *e.g.*, Heath *et al.*, 1974, or Muller, 1974), for gravity waves excited by the present mechanism have long wavelengths of the order of the width of the zonal shear flow. To discuss it in detail, however, it is necessary to solve a problem of vertical propagation of excited waves. It is left for later studies.

Acknowledgements

The author would like to express his thanks to Prof. T. Matsuno of Geophysical Institute of Tokyo University for his encouragements and discussions. He is also grateful to Prof. K. Gambo and all the staffs of the Meteorological Laboratory in the Geophysical Institute of Tokyo University for their support of this study and useful discussions. His thanks are extended to Dr. Yoshizaki in the Ocean Research Institute of Tokyo University for his discussions and criticisms.

The computations were performed by the use of the HITAC M-200H computer at the Computer Center of Tokyo University.

Appendix A: Finite difference scheme

We will present finite difference scheme, which was developed by Arakawa & Lamb (1981). At first, equations (2.3) and (2.4) are transformed to following forms:

$$\begin{aligned}
&\frac{\partial u}{\partial t}-q\hat{v}+\frac{\partial}{\varrho x}(K+\Phi)=0\,,\\
&\frac{\partial v}{\partial t}+q\hat{u}+\frac{\partial}{\partial y}(K+\Phi)=0\,,\\
&\frac{\partial h}{\partial t}+\frac{\partial \hat{u}}{\partial x}+\frac{\partial \hat{v}}{\partial y}=0\,,
\end{aligned} \tag{A.1}$$

where $(\hat{u},\ \hat{v})=(hu,\ hv)$ is the mass flux, $\Phi=h/Fr^2$, $K=(u^2+v^2)/2$, and viscous terms are dropped for simplicity.

Then, required finite-difference scheme which conserves total mass, energy, and potential enstrophy is given by

$$\begin{aligned}
&\frac{\partial}{\partial t}u_{i,\,j+1/2}-\alpha_{i,\,j+1/2}\hat{v}_{i+1/2,\,j+1}\\
&\quad-\beta_{i,\,j+1/2}\hat{v}_{i-1/2,\,j+1}-\gamma_{i,\,j+1/2}\hat{v}_{i-1/2,\,j}\\
&\quad-\delta_{i,\,j+1/2}\hat{v}_{i+1/2,\,j}+\varepsilon_{i+1/2,\,j+1/2}\hat{u}_{i+1,\,j+1/2}\\
&\quad-\varepsilon_{i-1/2,\,j+1/2}\hat{u}_{i-1,\,j+1/2}+1/d\\
&\quad\times[(K+\Phi)_{i+1/2,\,j+1/2}-(K+\Phi)_{i-1/2,\,j+1/2}]=0,
\end{aligned} \tag{A.2}$$

$$\begin{aligned}
&\frac{\partial}{\partial t}v_{i+1/2,\,j}+\gamma_{i+1,\,j+1/2}\hat{u}_{i+1,\,j+1/2}\\
&\quad+\delta_{i,\,j+1/2}\hat{u}_{i,\,j+1/2}+\alpha_{i,\,j-1/2}\hat{u}_{i,\,j-1/2}\\
&\quad+\beta_{i+1,\,j-1/2}\hat{u}_{i+1,\,j-1/2}+\phi_{i+1/2,\,j+1/2}\hat{v}_{i+1/2,\,j+1}\\
&\quad-\phi_{i+1/2,\,j-1/2}\hat{v}_{i+1/2,\,j-1}+1/d\\
&\quad\times[(K+\Phi)_{i+1/2,\,j+1/2}-(K+\Phi)_{i+1/2,\,j-1/2}]=0\,,
\end{aligned} \tag{A.3}$$

$$\begin{aligned}
&\frac{\partial}{\partial t}h_{i+1/2,\,j+1/2}+\frac{1}{d}[\hat{u}_{i+1,\,j+1/2}-\hat{u}_{i,\,j+1/2}\\
&\quad+\hat{v}_{i+1/2,\,j+1}-\hat{v}_{i+1/2,\,j}]=0\,,
\end{aligned} \tag{A.4}$$

where $d=\Delta x=\Delta y$ is the grid interval,

$$\hat{u}_{i,\,j+1/2}=\frac{1}{2}(h_{i+1/2,\,j+1/2}+h_{i-1/2,\,j+1/2})u_{i,\,j+1/2,\,j}, \tag{A.5}$$

$$\hat{v}_{i+1/2,\,j}=\frac{1}{2}(h_{i+1/2,\,j+1/2}+h_{i+1/2,\,j-1/2})v_{i+1/2,\,j}, \tag{A.6}$$

$$\begin{aligned}
\varepsilon_{i+1/2,\,j+1/2}=\frac{1}{24}&[q_{i+1,\,j+1}+q_{i,\,j+1}-q_{i,\,j}\\
&-q_{i+1,\,j}]\,,
\end{aligned} \tag{A.7}$$

$$\phi_{i+1/2,\,j+1/2}=\frac{1}{24}[-q_{i+1,\,j+1}+q_{i,\,j+1}+q_{i,\,j}-q_{i+1,\,j}], \tag{A.8}$$

$$\alpha_{i,\,j+1/2}=\frac{1}{24}[2q_{i+1,\,j+1}+q_{i,\,j+1}+2q_{i,\,j}+q_{i+1,\,j}], \tag{A.9}$$

$$\beta_{i,\,j+1/2}=\frac{1}{24}[q_{i,\,j+1}+2q_{i-1,\,j+1}+q_{i-1,\,j}+2q_{i,\,j}], \tag{A.10}$$

$$\gamma_{i,\,j+1/2}=\frac{1}{24}[2q_{i,\,j+1}+q_{i-1,\,j+1}+2q_{i-1,\,j}+q_{i,\,j}], \tag{A.11}$$

$$\delta_{i,\,j+1/2}=\frac{1}{24}[q_{i+1,\,j+1}+2q_{i,\,j+1}+q_{i,\,j}+2q_{i+1,\,j}], \tag{A.12}$$

$$q_{i,\,j}=\frac{\frac{1}{d}[u_{i,\,j-1/2}-u_{i,\,j+1/2}+v_{i+1/2,\,j}-v_{i-1/2,\,j}]}{\frac{1}{4}\left[\begin{array}{l}(h_{i+1/2,\,j+1/2}+h_{i-1/2,\,j+1/2}\\ \quad+h_{i-1/2,\,j-1/2}+h_{i+1/2,\,j-1/2})\end{array}\right]}, \tag{A.13}$$

$$K_{i+1/2,\,j+1/2}=\frac{1}{2}\cdot\frac{1}{2}(u^2{}_{i+1,\,j+1/2}+u^2{}_{i,\,j+1/2}+v^2{}_{i+1/2,\,j+1}+v^2{}_{i+1/2,\,j}). \tag{A.14}$$

In order to prove the conservation characteristics of this scheme, an attention should be given to grid points near the boundaries. To suffice the requirements of the conservation of total mass and total energy, it is adequate to set v-points at the rigid walls as shown Fig. A1, and $v=0$ at the walls. On the other hand, it is easy to derive that following forms for $q_{i,b1}$ and $q_{i,b2}$, which are potential vorticity on the walls, satisfy the conservation law of potential enstrophy:

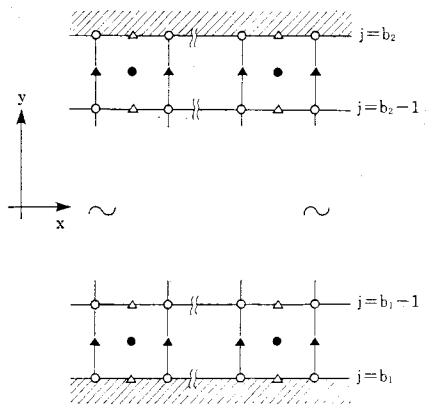

Fig. A1 Grid distribution of present model.

$$\frac{1}{2}(h_{i+1/2,\,B\pm1/2}+h_{i-1/2,\,B\pm1/2})\frac{\partial}{\partial t}q_{i,\,B}=-\frac{2}{d}\left[\frac{1}{12}\{(\hat{u}_{i+1,\,B\pm1/2}+\hat{u}_{i,\,B\pm1/2})(q_{i+1,\,B}-q_{i,\,B})+(\hat{u}_{i,\,B\pm1/2}+\hat{u}_{i-1,\,B\pm1/2})(q_{i,\,B}-q_{i-1,\,B})\pm(\hat{v}_{i+1/2,\,B\pm1}+\hat{v}_{i-1/2,\,B\pm1})(q_{i\pm B\pm1}-q_{i,\,B})\}\pm\frac{1}{24}\{(\hat{v}_{i\pm1/2,\,B\pm1}+\hat{u}_{i\pm1,\,B\pm1/2}+\hat{u}_{j,\,B\pm1/2})\times(q_{i\pm1,\,B\pm1}-q_{i,\,B})+(\hat{v}_{i\mp1/2,\,B\pm1}+\hat{u}_{i\mp1,\,B\pm1/2}-\hat{u}_{i,\,B\pm1/2})(q_{i\mp1,\,B\pm1}-q_{i,\,B})\}\right] \tag{A.15}$$

where $B=b1$ and $b2$ for the plus sign and the minus sign, respectively. This scheme (A.15) is used to calculate $q_{i,b1}$ and $q_{i,b2}$ in the inviscid case.

The scheme (A.15) is stable in a sense that square quantities such as the potential enstrophy and energy are finite and conserved. A little calculation shows, however, that (A.15) can be transformed as

$$\frac{1}{2}(h_{i+1/2,\,B\pm1/2}+h_{i-1/2,\,B\pm1/2})\frac{\partial q_{i,\,B}}{\partial t}=-q_{i,\,B}\frac{\partial}{\partial t}\frac{1}{2}(h_{i+1/2,\,B\pm1/2}+h_{i-1/2,\,B\pm1/2})+G(q,\hat{u},\hat{v}), \tag{A.16}$$

where G is a function of q, $\hat{u}$, and $\hat{v}$. If

$$\frac{\partial}{\partial t}(h_{i+1/2,\,B\pm1/2}+h_{i-1/2,\,B\pm1/2})<0, \tag{A.17}$$

(A.16) seems unstable. In the inviscid case of this paper, there is no problem because $q=-1$ initially everywhere in the domain and, thus, the right-hand side of (A.15) is always zero within the truncation and round-off errors.

On the other hand, however, q will vary physically with time in the viscous case, and the right-hand side of (A.15) is no longer zero due to the viscosity. Because (A.15) has the ambiguity in the stability property as seen in (A.16) and because it is hard to find out an appropriate definition of the viscous terms which should be added to the right-hand side of (A.15), we define $q_{i,b1}$ and $q_{i,b2}$ as

$$q_{i,B}=\frac{(u_{i,\,B\pm1/2}-u_{i,\,B\pm3/2}+v_{i+1/2,\,B\pm1}-v_{i-1/2,\,B\pm1})/d}{(h_{i+1/2,\,B\pm1/2}+h_{i-1/2,\,B\pm1/2})/2}, \tag{A.18}$$

i.e.,

$$q_{i,\,B}=\frac{(\nabla\times V)_{i,\,B\pm1}}{(h)_{i,\,B\pm1/2}} \tag{A.19}$$

Instead of (A.15), we use above scheme in the

viscous run.

Although scheme (A.18) destroys the conservation law of the total potential enstrophy, the effect of the destruction on numerical solutions is found to be small not only in the inviscid case but also in the viscous case. Thus, we regard numerical solutions as physical solutions.

Appendix B: Energy equations

Because energy equations are rather strange form, we present detailed derivation of them.

The total kinetic energy is

$$K=\frac{1}{2}\int_{-1/2}^{1/2}\overline{h(u^2+v^2)}dy$$
$$=\frac{1}{2}\int_{-1/2}^{1/2}\{\bar{h}(\bar{u}^2+\bar{v}^2)+2(\overline{h'u'}\bar{u}+\overline{h'v'}\bar{v})\}dy$$
$$+\frac{1}{2}\int_{-1/2}^{1/2}\overline{(\bar{h}+h')(u'^2+v'^2)}dy\,. \qquad \text{(B.1)}$$

The mean kinetic energy $\bar{K}$ and the disturbance energy K' are defined by

$$\bar{K}=\frac{1}{2}\int_{-1/2}^{1/2}\{\bar{h}(\bar{u}^2+\bar{v}^2)+2(\overline{h'u'}\bar{u}+\overline{h'v'}\bar{v})\}dy\,, \qquad \text{(B.2)}$$

$$K'=\frac{1}{2}\int_{-1/2}^{1/2}\overline{(\bar{h}+h')(u'^2+v'^2)}dy\,. \qquad \text{(B.3)}$$

Instead of the zonal average, we can use a weighted mean velocity $\tilde{V}$ defined as

$$\tilde{V}=\frac{\overline{hV}}{\bar{h}}\,,$$

and a deviation from it,

$$\dot{V}=V-\tilde{V}\,,$$

to construct energy equations (ex. Eliassen and Kleinschmidt, 1957). The energy equations expressed by $\tilde{V}$ and $\dot{V}$ have two advantages: K_a is implicitly included in the 'mean' energy, and transformation terms are little simpler. Those equations are, however, essentially equivalent to the present equations, and the strange transformation (B.17) does not disappeared even in those equations. Moreover, the importance of K_a would be overlooked. Thus, we use the ordinary zonal average.

The total available potential energy is

$$P=\frac{1}{F_r^2}\cdot\frac{1}{2}\int_{-1/2}^{1/2}\left(h-\int_{-1/2}^{1/2}\bar{h}dy\right)^2dy$$
$$\frac{1}{F_r^2}\cdot\frac{1}{2}\int_{-1/2}^{1/2}(h-1)^2dy\,. \qquad \text{(B.4)}$$

The mean available potential energy $\bar{P}$ and the disturbance potential energy P' are defined by

$$\bar{P}=\frac{1}{F_r^2}\cdot\frac{1}{2}\int_{-1/2}^{1/2}(\bar{h}-1)^2dy\,, \qquad \text{(B.6)}$$

$$P'=\frac{1}{F_r^2}\cdot\frac{1}{2}\int_{-1/2}^{1/2}\overline{h'^2}dy\,. \qquad \text{(B.6)}$$

As a preparation of derivation of energy equations, we derive the equations of time change of momentum. Zonal average of (2.3) and (2.4) are

$$\frac{\partial}{\partial t}\bar{V}+\bar{v}\frac{\partial}{\partial y}\bar{V}+\overline{\left(u'\frac{\partial}{\partial x}+v'\frac{\partial}{\partial y}\right)V'}$$
$$+\frac{1}{F_r^2}\nabla\bar{h}=\frac{1}{R_e}\bar{F}\,, \qquad \text{(B.7)}$$

$$\frac{\partial\bar{h}}{\partial t}+\frac{\partial}{\partial y}\bar{h}\bar{v}+\frac{\partial}{\partial y}\overline{h'v}=0\,. \qquad \text{(B.8)}$$

Subtracting (B.7) and (B.8) from (2.3) and (2.4) respectively, we obtain

$$\frac{\partial V'}{\partial t}+\left(u'\frac{\partial}{\partial x}+v'\frac{\partial}{\partial y}\right)V'-\overline{\left(u'\frac{\partial}{\partial x}+v'\frac{\partial}{\partial y}\right)V'}$$
$$+v'\frac{\partial\bar{V}}{\partial y}+\left(\bar{u}\frac{\partial}{\partial x}+\bar{v}\frac{\partial}{\partial y}\right)V'+\frac{1}{F_r^2}\nabla h'$$
$$=\frac{1}{R_e}F'\,, \qquad \text{(B.9)}$$

$$\frac{\partial h'}{\partial t}+\frac{\partial}{\partial x}(h'u'+\bar{h}u'+h'\bar{u})$$
$$+\frac{\partial}{\partial y}(h'v'+\bar{h}v'+h'\bar{v}-\overline{h'v'})=0\,. \qquad \text{(B.10)}$$

Multiplying (B.7) and (B.8) by $\bar{h}$ and $\bar{V}$ respectively, and adding the results, we obtain

$$\frac{\partial}{\partial t}\bar{h}\bar{V}+\frac{\partial}{\partial y}(\bar{h}\bar{V}\bar{v}+\bar{h}\overline{V'v'})\,.$$
$$=\overline{V'\nabla\cdot(\bar{h}V')}-\bar{V}\frac{\partial\overline{h'v'}}{\partial y}-\frac{\bar{h}}{F_r^2}\Delta\bar{h}+\frac{\bar{h}\bar{F}}{R_e}\,. \qquad \text{(B.11)}$$

This is the equation of zonally averaged momentum.

Subtracting (B.11) from the equation of total momentum, which is written as

$$\frac{\partial}{\partial t}hV+\frac{\partial}{\partial x}(huV)+\frac{\partial}{\partial y}(hvV)$$
$$+\frac{h}{F_r^2}\nabla h=\frac{h}{R_e}F\,, \qquad \text{(B.12)}$$

and averaging zonally, we obtain

$$\frac{\partial}{\partial t}\overline{h'V'}+\frac{\partial}{\partial y}(\overline{h'V'v'}+\overline{h'V'}\bar{v}+\bar{V}\overline{h'v'})$$

$$= -\overline{V'\bar{V}\cdot(\bar{h}V')} + \bar{V}\frac{\partial}{\partial y}\overline{h'v'} - \frac{1}{F_r^2}\overline{h'\bar{V}h'} + \frac{1}{R_e}\overline{h'F'}. \quad \text{(B.13)}$$

This is the equation of averaged disturbance momentum.

Then, multiplying (B.7) and (B.11) by $\bar{h}\bar{V}/2$ and $\bar{V}/2$ respectively, multiplying (B.7) and (B.13) by $\overline{h'V'}$ and $\bar{V}$ respectively, adding the results, and integrating with y, we obtain the equation of the mean kinetic energy as

$$\frac{\partial}{\partial t}\bar{K} = -[\bar{K}K'] - [\bar{K}\bar{P}] - [\bar{K}P'] - \bar{D}, \quad \text{(B.14)}$$

where the transformation terms $[\bar{K}K']$, $[\bar{K}\bar{P}]$, and $[\bar{K}P']$ are defined as

$$[\bar{K}K'] = -\int_{-1/2}^{1/2}\overline{hv'V'}\cdot\frac{\partial\bar{V}}{\partial y}dy + \int_{-1/2}^{1/2}\overline{h'V'}\cdot\overline{\left(u'\frac{\partial}{\partial x}+v'\frac{\partial}{\partial y}\right)V'}dy, \quad \text{(B.15)}$$

$$[\bar{K}\bar{P}] = -\frac{1}{F_r^2}\int_{-1/2}^{1/2}\bar{h}\frac{\partial}{\partial y}(\bar{h}\bar{v}+\overline{h'v'})dy, \quad \text{(B.16)}$$

$$[\bar{K}P'] = \frac{1}{F_r^2}\int_{-1/2}^{1/2}\overline{h'\frac{\partial h'\bar{v}}{\partial y}}dy, \quad \text{(B.17)}$$

$$\bar{D} = \frac{1}{R_e}\int_{-1/2}^{1/2}(\bar{h}\bar{V}\bar{F}+\overline{h'V'}\cdot\bar{F}+\overline{h'F'}\cdot\bar{V})dy. \quad \text{(B18)}$$

Meanings of transformations will be explained later.

Since the last term of the integrand of (B.2) plays an important role as shown in S1, we divide the mean kinetic energy $\bar{K}$ into two parts:

$$\bar{K} = K_z + K_a, \quad \text{(B.19)}$$

where

$$K_z = \frac{1}{2}\int_{-1/2}^{1/2}\bar{h}(\bar{u}^2+\bar{v}^2)dy \quad \text{(B.20)}$$

expresses the mean kinetic energy arising from only the zonal averaged quantities, and

$$K_a = \int_{-1/2}^{1/2}(\overline{h'u'}\bar{u}+\overline{h'v'}\bar{v})dy \quad \text{(B.21)}$$

is interpreted as the additional part of the mean kinetic energy due to the disturbance surface displacement. Then, equation (B.14) is divided as follows:

$$\frac{\partial}{\partial t}K_z = -[K_zK'] - [K_zK_a] - [\bar{K}\bar{P}] - D_z, \quad \text{(B.21)}$$

$$\frac{\partial}{\partial t}K_a = -[K_aK'] + [K_zK_a] - [\bar{K}P'] - D_a, \quad \text{(B.23)}$$

where

$$[K_zK'] = -\int_{-1/2}^{1/2}\bar{h}\overline{v'V'}\cdot\frac{\partial\bar{V}}{\partial y}dy, \quad \text{(B.24)}$$

$$[K_zK_a] = -\int_{-1/2}^{1/2}\left\{\overline{h'v'}\bar{V}\cdot\frac{\partial\bar{V}}{\partial y} + \bar{V}\cdot\overline{V'\bar{V}(\bar{h}V')}\right\}dy, \quad \text{(B.25)}$$

$$[K_aK'] = -\int_{-1/2}^{1/2}\left\{\overline{h'v'V'}\cdot\frac{\partial\bar{V}}{\partial y} - \overline{h'V'}\cdot\overline{\left(u'\frac{\partial}{\partial x}+v'\frac{\partial}{\partial y}\right)V'}\right\}dy, \quad \text{(B.26)}$$

$$D_z = \frac{1}{R_e}\int_{-1/2}^{1/2}\bar{h}\bar{V}\cdot\bar{F}dy, \quad \text{(B.27)}$$

$$D_a = \frac{1}{R_e}\int_{-1/2}^{1/2}(\overline{h'V'}\cdot\bar{F}+\overline{h'F'}\cdot\bar{V})dy, \quad \text{(B.28)}$$

The time rate of change of the disturbance kinetic energy K' is obtained by subtracting (B.14) from the equation of the total kinetic energy, and is written as

$$\frac{\partial}{\partial t}K' = [\bar{K}K'] - [K'P'] - D', \quad \text{(B.29)}$$

where

$$[K'P'] = \frac{1}{F_r^2}\int_{-1/2}^{1/2}\overline{h\bar{V}'\cdot\bar{\nabla}h'}dy, \quad \text{(B.30)}$$

$$D' = \frac{1}{R_e}\int_{-1/2}^{1/2}\overline{hV'\cdot F'}dy, \quad \text{(B.31)}$$

The rate of time change of $\bar{P}$ and P' are obtained from (B.8) and (B.10) respectively, and are written as

$$\frac{\partial}{\partial t}\bar{P} = [\bar{K}\bar{P}], \quad \text{(B.32)}$$

$$\frac{\partial}{\partial t}P' = [K'P'] + [\bar{K}P'], \quad \text{(B.33)}$$

The transformation $[\bar{K}K']$ represents a conversion from the mean kinetic energy $\bar{K}$ into the disturbance kinetic energy K' and is a sum of the conversion by the Reynolds stress and the higher order correlation. The transformation $[\bar{K}\bar{P}]$, $[K'P']$, and $[\bar{K}P']$ are the elements of total $[KP]$ transformation which manifests the work of the flow to raise the surface against the gravity.

The $[K_zK_a]$ transformation represents the inner conversion between the constituents K_z and

K_a of the mean kinetic energy $\bar{K}$. Transformations $[K_zK']$ and $[K_aK']$ are the elements of the $[\bar{K}K']$. $\bar{D}$, D', D_z, and D_a represents the dissipation rates of the kinetic energy $\bar{K}$, K' K_z, and K_a, respectively.

Appendix C: Derivation of viscous terms

In cases of viscous fluids with a free surface as a shallow water, we must include effects of the free surface into stress tensor of a viscous term. It comes from both facts that a volume element on the free surface feels no stress from the out side of the fluid and that we treat the fluid only as a set of columns. We will take such effects on stress tensor into account.

In general cases, stress tensor is written as

$$P_{ij}=-P\delta_{ij}+2\eta\left(e_{ij}-\frac{1}{3}e_{ll}\delta_{ij}\right), \tag{C.1}$$

where δ_{ij} is the Kronecker's delta and is defined as

$$\delta_{ij}=\begin{cases}1 & \text{for } i=j\\ 0 & \text{for } i\neq j,\end{cases} \tag{C.2}$$

η is the first coefficient of the viscosity, and

$$e_{ij}=\frac{1}{2}\left(\frac{\partial u_i}{\partial x_j}+\frac{\partial u_j}{\partial x_i}\right) \tag{C.3}$$

is the rate of strain tensor. In this appendix, we use subscripts i, $j=1$, 2, and 3 to indicate the x, y, and z components respectively, for simplifying tensor expression.

The equation of momentum is written as

$$\frac{\partial}{\partial t}\iiint_V \rho u_i dV=\iint_S P_{ij}n_j dS-\iint_S \rho u_i u_j n_j dS+\iiint_V \rho K_i dV, \tag{C.4}$$

where V is a volume enclosed by a surface S, n_j is a j-th component of the normal vector of S, and K_i is a body force.

Since, in case of a shallow water, hydrostatic balance is assumed, and both u_1 and u_2 are independent of x_3, we can integrate (C.4) for a fixed column which has a cross section S_c and a periphery C to obtain.

$$\frac{\partial}{\partial t}\iint_{S_c} hu_n dS_c=\oint_c P_{mn}ds-\oint_c hu_m u_n ds, \tag{C.5}$$

where P_{mn} is defined as

$$P_{mn}=-\frac{1}{2}gh^2\delta_{mn}+2\nu he_{mn}, \tag{C.6}$$

where ν is the coefficient of kinetic viscosity,

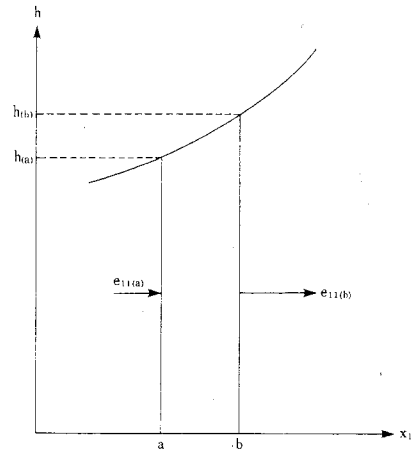

Fig. C1 Schematic representation of viscous force. At $x_1=a$, depth is $h(a)$ and stress is $2e_{11}(a)$. At $x_1=b=a+\Delta x$, depth is $h(b)$ and stress is $2e_{11}(b)$.

$$e_{mn}=\frac{1}{2}\left(\frac{\partial u_m}{\partial x_n}+\frac{\partial u_n}{\partial x_m}\right) \tag{C.7}$$

and m, $n=1$, 2. We used the facts that e_{ll} in the right-hand side of (C.1) becomes zero from the equation of continuity (2.4) and that there is no momentum flux through the bottom or the surface of the shallow water.

Then, transformation from the integral equation (C.5) to a differential equation gives the required equation as

$$\frac{\partial}{\partial t}hu_m=\frac{\partial}{\partial x_n}\left\{\frac{gh^2}{2}\delta_{mn}+\nu h\left(\frac{\partial u_m}{\partial x_n}+\frac{\partial u_n}{\partial x_m}\right)\right\}-\frac{\partial}{\partial x_n}(hu_m u_n). \tag{C.8}$$

Thus, the x_1 and x_2 component of the viscosity term of (C.8) are the right-hand sides of (3.6) and (3.7), respectively. Of course, (3.6) and (3.7) are reduced to the ordinary Laplacian forms if h is a constant.

Now, it is easy to derive them physically. We will confine ourselves to considering only one direction of the stress tensor for simplicity (see Fig. C1). The momentum flux by stress per unit area is $2e_{11}$. Thus, the total momentum flux through the left-hand side of the column at $x_1=a$ is $2e_{11(a)}h_{(a)}$, and the flux through the right-hand side is $2e_{11(b)}h_{(b)}$. Because the force which acts the column is the divergence of the momentum flux, the viscous term should have the form as

$$F_{(x=a)}=\lim_{\Delta x\to 0}\frac{h_{(a+\Delta x)}\cdot 2e_{11(a+\Delta x)}-h_{(a)}\cdot 2e_{11(a)}}{\Delta x}$$

$$=\left[\frac{\partial}{\partial x}(2he_{11})\right]_{x=a}. \qquad (C.9)$$

If we extend above discussion to all directions, we will get the same terms as (3.6) and (3.7).

References

Arakawa, A., and V. R. Lamb, 1981: A potential enstrophy and energy conserving scheme for the shallow water equations. *Mon. Wea. Rev.*, **109**, 37-51.

Blumen, W., P. G. Drazin and D. F. Billings, 1975: Shear layer instability for an inviscid compressible fluid. Part 2. *J. Fluid Mech.*, **71**, 305-316.

Drazin, P. G., and A. Davey, 1977: Shear layer instability of an inviscid compressible fluid. Part 3. *J. Fluid Mech.*, **82**, 255-260.

Eliassen, A., and E. Kleinschmidt, 1957: 'Dynamic Meteorology' in Handbuch der Physik, Springer, Berlin, **48**, 1-154.

Heath, D. F., E. Hilsenrath, A. J. Krueger, W. Nordberg, C. Prabhakara and J. S. Theon, 1974: In 'Structure and Dynamics of the Upper Atmosphere', F. Verniani (ed.), Elsevier Scientific Publ. Co., 131-198.

Muller, H. G., 1974: ibid., 347-388.

Satomura, T., 1981a: An investigation of shear instability in a shallow water. *J. Meteor. Soc. Japan*, **59**, 148-167.

———, 1981b: Supplementary note on shear instability in a shallow water. *ibid.*, **59**, 168-171.

浅水のシアー不安定に関する研究

第II部 数 値 実 験

里 村 雄 彦

東京大学理学部地球物理学教室

浅水の水路モデルを用い，シアーのある流れで有限振幅となった不安定重力波の振舞いを数値的に調べた。フルード数は5に固定し，非粘性の場合と粘性のある場合（レイノルズ数 Re=3000）の両方について計算した。

非粘性の場合，最初に発達する波は線型理論で求めたのと同じ成長率と構造を持っていた。この波は，線型理論の場合と同じく，$\overline{h'u'}\bar{u}$ からエネルギーを得ている。

粘性がある場合，波のエネルギーは準定常状態に達し，運動量は恒久的な混合を受けることを示した。そのときのエネルギーの流れは，壁付近の粘性⟶平均の運動エネルギー⟶波の運動エネルギー⟶波に作用する粘性，となっている。

準定常状態になった後も時間積分を続けると，波のエネルギーは振動を始めた。準定常状態の安定性を調べた結果，基本波の半分の波数を持つモードが不安定となって振動を起こすことがわかった。